Applied Catalysis B: Environmental 258 (2019) 118032

Contents lists available at ScienceDirect

Applied Catalysis B: Environmental

journal homepage: www.elsevier.com/locate/apcatb

Investigation of an irreversible NOx storage degradation Mode on a Pd/BEA passive NOx adsorber

Yuntao Gu, Ryan P. Zelinsky, Yu-Ren Chen, William S. Epling*

Department of Chemical Engineering, University of Virginia, Charlottesville, VA, 22903, United States

ARTICLE INFO

Keywords:
Cold start
Engine emissions
Passive NOx adsorber
NOx storage
Catalyst deactivation
Palladium zeolite catalyst

ABSTRACT

Passive NOx adsorbers (PNAs) are a proposed solution for cold start NOx emissions, via low temperature NOx trapping and subsequent release at a temperature where downstream NOx reduction catalysts are active. Pd/zeolites have been reported to have significant NOx storage capacities. However, their real exhaust compatibility has not been completely evaluated. In this work, Pd/BEA was used to study the mechanism of an observed PNA degradation. NO adsorption, NO and CO co-adsorption and temperature programmed desorption/oxidation were performed on a series of differently aged Pd/BEA catalysts to evaluate the NOx storage capacity and desorption temperature. An irreversible NOx storage degradation mode caused by low temperature CO exposure was observed. H_2 temperature programmed reduction results indicate this irreversible degradation can be attributed to the loss of Pd^{2+}. Additionally, STEM images revealed Pd particle migration/agglomeration after hydrothermal aging and CO/H_2 exposure. Larger particles, formed during CO exposure, lead to the irreversible degradation.

1. Introduction

There has been significant progress in automobile NOx abatement technologies [1–6]. Current state-of-the-art selective catalytic reduction (SCR) catalysts designed for diesel NOx abatement can meet currently required regulation limits, and have proven hydrothermally stable [7–11]. However, progressively more stringent emission regulations as well as fuel economy requirements drive the need for further advancement in exhaust after-treatment technologies [3]. Notably, the development of advanced compression ignition technologies usually results in a lower exhaust temperature [12]. To meet these even more stringent regulations, and the challenges associated with lower exhaust temperatures, low-temperature catalysis remains a research focus [12–14]. The remediation of “cold start” NOx, namely NOx emitted before the after-treatment system is warmed up enough to achieve high pollutant conversions, remains challenging. Arguably, the SCR catalytic activity at low temperatures can be improved with new catalyst designs and formulations. However, urea decomposition, as the current in application ammonia source, occurs at temperatures above 180 °C [15].

Passive NOx adsorbers (PNAs) are proposed as one of the solutions to help address cold start NOx emissions [15–18]. PNAs can trap NOx at low temperatures, thereby removing NOx during cold start. An appropriate NOx desorption temperature window is also key to ultimately reducing NOx, since desorption at too low of a temperature will allow it to slip through the downstream SCR catalyst unconverted [16]. PNA candidate materials have been evaluated. Crocker’s group investigated a series of Pd- and Pt-promoted alumina and ceria/zirconia PNAs. They studied formulation performance dependency and provided insight into the NOx trapping and release characteristics of these model systems [19–22]. Theis et al. looked into the exhaust composition effects on the NOx adsorption and desorption behavior of Pd promoted ceria/zirconia [23–26]. Chen et al. have shown that Pd/zeolite systems performed significantly better than ceria-based PNAs in terms of NOx storage capacity per unit mass of precious metal, NOx desorption temperature and their real exhaust compatibilities [27]. Since then, Pd/BEA, Pd/ZSM-5 and Pd/SSZ-13 have attracted significant attention [28–34]. In terms of the NOx trapping mechanism, it is believed that ion-exchanged cationic Pd species are the key adsorption sites. For example, Zheng et al. and Ryou et al. have tested and characterized a series of Pd/zeolite systems and concluded that Pd cations are the dominant trapping sites and a thermal or hydrothermal treatment during catalyst synthesis plays an important role in forming those sites via Pd dispersion into the zeolite system [35–37]. In addition, using a modified ion-exchange method, Khivantsev et al. were able to achieve a 1:1 NOx-to-Pd ratio, thus maximizing the atomic utilization [38].

Because the PNA is the most upstream after-treatment system component, or integrated with the most upstream component, these trapping sites will be exposed to a variety of exhaust gas compositions.

* Corresponding author.
E-mail address: wse2t@virginia.edu (W.S. Epling).

https://doi.org/10.1016/j.apcatb.2019.118032
Received 18 February 2019; Received in revised form 10 June 2019; Accepted 29 July 2019
Available online 30 July 2019

Therefore, to better characterize NOx trapping and release, as well as understand potential degradation modes, this catalyst needs to be evaluated during and after exposure to exhaust gas components. Effects of O_2, H_2O and CO_2 have been studied for example. It was found that O_2 is key to high NOx storage capacity under dry conditions due to the formation of nitrate and nitrite species [39], however, CO_2 does not have a significant impact on the NOx storage capacity of Pd/BEA neither does it affect NOx desorption [40]. For Pd-SSZ-13, H_2O inhibits NOx adsorption by strongly interacting with Bronsted sites at low temperatures, thus resulting in a significant decrease in NOx storage capacity [27]. The effect of CO has also been studied. Vu et al. found that CO can shift NOx desorption temperatures to a more ideal range [40], and in a recently published work, Ryou et al. also found that CO can reduce Pd cations and accelerate particle sintering under rich conditions [41].

In this paper, Pd/BEA was chosen as a model PNA, and its NOx trapping and desorption characteristics were evaluated under simulated exhaust conditions, with the emphasis on the impact of CO. An irreversible NOx storage degradation mode was observed and a mechanistic explanation provided.

2. Experimental methods

2.1. Catalyst synthesis

A series of Pd impregnated BEA zeolite catalysts as well as the proton form catalysts/adsorbers were synthesized and evaluated in this study. Pd/BEA was chosen based on its previous use in the literature [17] as well as its use as a hydrocarbon trap, which can simultaneously trap NO. All Pd-containing catalysts were prepared via incipient wetness impregnation, and some of the resulting powder was used to washcoat cordierite monolith substrates. The ammonium form of BEA zeolite with a 12.5 Si/Al ratio was purchased from Zeolyst Inc. A three-step calcination process (80 °C for 2 h, 105 °C for 10 h and 500 °C for 4 h with a ramp rate of 1 °C/min) was used to transform the BEA zeolite into proton form before introducing Pd. $Pd(NO_3)_2$ dissolved in nitric acid was selected as the precursor, which was purchased from Sigma Aldrich. Deionized water was used to dilute the Pd solution, such that the volume of Pd containing solution was the same as the pore volume of the zeolite, and to achieve 1 wt.% or 0.5 wt.% of Pd. Immediately following the calcination to make the proton form, the $Pd(NO_3)_2$ solution was drop wise added with rigorous stirring and mixing. After Pd was introduced, the same calcination process was repeated.

A slurry was prepared to washcoat 300 cpsi cordierite monolith, which contained a large portion of freshly calcined catalyst powder, deionized water and an alumina colloidal binder solution purchased from Nyacol Nano Technologies, Inc. The zeolite-to-alumina mass ratio was 8:1. Before washcoating, the slurry was agitated and ball-milled with ceramic beads overnight. Monolithic cordierite substrates were trimmed to fit a 0.5-inch ID quartz tube, then dipped into the prepared slurry and dried with flowing air at 120 °C. After drying, the mass of the wash-coated monolith cores was measured to calculate the washcoat loading, and this process was repeated several times until a 1 g/in^3 washcoat loading was achieved. Finally, the three-step calcination process was repeated.

The freshly calcined catalysts were hydrothermally aged by exposing the catalysts in either powder form or monolith form to a gas mixture of 10% O_2 and 10% H_2O balanced by N_2 for 16 h at a space velocity of 30,000 h^{-1}. For experiments using the powder form, a monolith equivalent space velocity of 30,000 h^{-1} was maintained. This assumes a uniform powder distribution on the same monolith substrate with a 1 g/in^3 washcoat loading. The hydrothermal aging temperature for the samples evaluated ranged from 600 to 800 °C with a 50 °C increment. Samples are labeled as Pd/BEA-600HTA, Pd/BEA-650HTA and so on.

2.2. Catalyst characterization

A Pd weight lading of 1 wt.% was confirmed by ICP-OES analysis at Galbraith Laboratories and EDS analysis on a FEI-Titan transmission electron microscope with an X-ray detector. Crystallinity of the catalysts after calcination and hydrothermal aging were investigated via X-ray diffraction (XRD) using a PANalytical X'Pert Pro multi-purpose diffractometer. Cu Kα X-ray source and a vertical circle theta:theta goniometer with an incident radius of 240 mm were used. Scanning transmission electron micrographs (STEM) were collected on a FEI Titan transmission electron microscope in HAADF mode. H_2 temperature programmed reduction (H_2-TPR) data were collected using a Micromeritics AutoChem 2920 system. Powder samples were used for the characterization to avoid interference from the monolith support.

2.3. Catalyst evaluation

The low-temperature NOx storage experiments were conducted in a 0.5-inch quartz tube reactor horizontally placed in a tubular furnace purchased from Thermo Fisher. To simulate diesel exhaust conditions, a gas mixture of 10% O_2, 5% H_2O and 200 ppm NO was chosen as a basic gas composition, and 200 ppm CO were added in some cases to evaluate NO and CO co-adsorption. All the gases were balanced by N_2. All gas components were purchased from Praxair except N_2, which was purified from compressed air by a Parker N_2 generator. H_2O was injected using a Bronkhorst controlled evaporator mixer (CEM). The total flowrate was controlled to maintain a 30,000 h^{-1} space velocity under standard conditions. 80 °C was chosen as the adsorption temperature, consistent with previous work [40]. Before exposing the catalysts to the simulated exhaust described above, the samples were exposed to 10% O_2 and balance N_2. Low-temperature NOx adsorption experiments were initiated by a simultaneous switch of two four-way valves located upstream and downstream of the reactor. The reactor temperature was measured by a K-type thermocouple inserted into the reactor along the axial direction at the downstream end of the monolith. The reactor outlet gas composition was measured and recorded by an MKS IR analyzer, MG2030. After the PNA was saturated, a subsequent temperature programmed desorption (TPD) experiment was initiated by linearly ramping the reactor temperature from 80 to 600 °C with a ramp rate of 100 °C/min and the same gas composition as the adsorption phase. When the reactor temperature reached 600 °C, the gas composition was switched to 10% O_2 balanced by N_2. This pretreatment gas mixture was simply used to establish a consistent strating surface for each following experiment.

Between each low-temperature NOx storage experiment, a high-temperature oxidative pretreatment was conducted by flowing 10% O_2 balanced by N_2 at 600 °C for 45 min if not otherwise specified. A H_2 pretreatment and NO_2 pretreatment were also conducted in some cases by flowing 5% H_2 balanced by N_2 or 1000 ppm NO_2, 500 ppm NO and 10% O_2 at 600 °C. Samples that have gone through H_2 and NO_2 pretreatments are labeled as H_2 reduced and NO_2 pretreated, respectively. The sequence of the basic set of experiments is described in Table 1. More details of specific experiments are listed in Table 2.

3. Results and discussion

3.1. X-Ray diffraction

XRD powder diffraction patterns of freshly calcined Pd/BEA samples as well as an H/BEA sample are shown in Fig. 1 **A**. Apart from the BEA morphology observed at 2 θ = 21.9° and 2 θ = 22.1° in all three samples, PdO particles coexist [42] in Pd impregnated samples even at 0.5 wt.% Pd loading, captured by diffraction features at 2 θ = 33.8° 54.6°. This result indicates that a significant portion of Pd introduced during catalyst synthesis has not been ion-exchanged, thus forming particles with an average size of 6 nm after calcination, based on

Table 1
Experiment protocols used to quantify NOx storage capacity for each hydrothermally treated sample.

Experiment	Exhaust composition	Temperature Profile
O_2 treatment	10% O_2 and N_2 balance	600 °C
Test cycle 1	10% O_2, 5% H_2O, 200 ppm NO and N_2 balance	10 °C/min ramp to 600 °C
O_2 treatment	10% O_2 and N_2 balance	600 °C
Test cycle 2	10% O_2, 5% H_2O, 200 ppm NO, 200 ppm CO and N_2 balance	10 °C/min ramp to 600 °C
O_2 treatment	10% O_2 and N_2 balance	600 °C
Test cycle 3	10% O_2, 5% H_2O, 200 ppm NO, 200 ppm CO and N_2 balance	10 °C/min ramp to 600 °C
O_2 treatment	10% O_2 and N_2 balance	600 °C
Test cycle 4	10% O_2, 5% H_2O, 200 ppm NO, 200 ppm CO and N_2 balance	10 °C/min ramp to 600 °C
O_2 treatment	10% O_2 and N_2 balance	600 °C
Test cycle 5	10% O_2, 5% H_2O, 200 ppm NO and N_2 balance	10 °C/min ramp to 600 °C
H_2 treatment	5% H_2 and N_2 balance	600 °C
Test cycle 6	10% O_2, 5% H_2O, 200 ppm NO and N_2 balance	10 °C/min ramp to 600 °C
O_2 treatment	10% O_2 and N_2 balance	600 °C
Test cycle 7	10% O_2, 5% H_2O, 200 ppm NO and N_2 balance	10 °C/min ramp to 600 °C

Scherrer equation calculations. The particle size agrees with the observation from STEM images, which is discussed later. Researchers from PNNL looked into the pH effect on the ion-exchange level when impregnating Pd into small pore zeolites, and concluded that higher pH and ammonium form zeolites are key to atomic dispersion of Pd [38]. An acidic environment was maintained when preparing the catalysts for this NOx storage study, which may explain the low ion-exchange level and initial existence of Pd/PdO particles.

Pd/BEA PNAs were exposed to high temperatures to evaluate hydrothermal stability. Previous research has shown that exposing BEA zeolites to high water content at high enough temperature can severely damage zeolite crystallinity via dealumination [43]. As is shown in Fig. 1 **B**, the main BEA feature at around $2\theta = 22.1^{\circ}$ remained even with the hydrothermal aging temperature as high as 800 °C, whereas another BEA feature at $2\ \theta = 7.74^{\circ}$ disappeared after hydrothermal aging even at 600 °C. This result demonstrates that BEA morphology experiences a long-range structural collapse while partially maintaining the BEA crystal structure within a shorter range. Since during the NOx adsorption and TPD experiments the temperature never exceeded 650 °C, it is assumed that the local BEA morphology and the zeolite ring structures remained throughout. With the increase in hydrothermal aging temperature, the Pd features at $2\theta = 40.2^{\circ}$ and 47.1° grew and the PdO features at $2\theta = 33.8^{\circ}$ and 54.6° shrunk. This could be due to the sintering of the extra-framework Pd, forming particles with an average size of 12 nm and Pd^{2+} ion exchanging during the hydrothermal aging process, which consumes PdO to facilitate protonolysis [44].

3.2. NO adsorption and H_2-TPR

Selected NOx TPD profiles from a series of experiments following the testing protocol described in the experimental section are shown in Fig. 2. TPD data sets for a 600 °C hydrothermally aged sample (Pd/BEA-600HTA) and a 750 °C hydrothermally aged sample (Pd/BEA-750HTA) are plotted in Fig. 2 **A** and Fig. 2 **B**, respectively. The desorption profile of fresh Pd/BEA-600HTA when CO is absent in the gas stream consists of a major peak at around 120 °C, a shoulder at around 200 °C and a minor feature at around 430 °C. The NOx-to-Pd ratio was calculated based on the amount adsorbed during the NOx adsorption phase. The 0.32 ratio obtained is low compared to other reported values [16,27]. Furthermore, the NOx desorption temperature is not satisfactory with most of the NOx desorbing below 200 °C. However, when CO was introduced into the gas stream, the desorption feature at 120 °C shifted to 200 °C and the minor feature at around 430 °C remained unaffected. This behavior has been previously reported in multiple Pd-zeolite systems, but the actual mechanism has yet to be determined [25,32,40]. Two of the most convincing mechanisms are the reduction of Pd strengthening the NO-Pd bond and the formation of a NO-Pd(II) − CO like surface intermediate [16,39,45]. Apart from the desorption temperature shift, the addition of CO into the gas stream also led to a slight decrease in NOx uptake. Note, no N_2O was observed during these or any of the experiments. The first repetition of the NO and CO co-adsorption experiment did not show a significant difference other than a further decreased NOx-to-Pd ratio. Further repetition of the NO and CO co-adsorption experiments were conducted, of which the TPD profiles are not shown because no changes were observed, and there were no more changes in the NOx-to-Pd ratio. Lastly, NO adsorption was performed in the absence of CO, after the consecutive NO and CO co-adsorption experiments, which is labeled in Fig. 2 **A** as “After CO Exposure”. The TPD profile has the same desorption characteristics as those prior to CO exposure, indicating no changes of storage site distribution before and after CO exposure, i.e. the changes observed with CO exposure were reversible in this case.

For the sample that was hydrothermally aged at a higher temperature, the Pd/BEA-750HTA sample, prior to CO exposure, “Fresh Sample”, there is a significant increase in NOx adsorption capacity

Table 2
NO adsorption and desorption experiment protocol used to test the CO-exposed and NO_2-regenerated samples after hydrothermal treatment.

Experiment	Exhaust composition	Temperature profile
O_2 treatment	10% O_2 and N_2 balance	600 °C
Test cycle 1	10% O2, 5% H2O, 200 ppm NO and N_2 balance	10 °C/min ramp to 600 °C
O_2 treatment	10% O_2 and N_2 balance	600 °C
Test cycle 2	10% O_2, 5% H_2O, 200 ppm NO, 200 ppm CO and N_2 balance	10 °C/min ramp to 200 °C
O_2 treatment	10% O_2 and N_2 balance	600 °C
NO_2 treatment	800 ppm NO_2, 800 ppm NO, 10% O_2 and N_2 balance	600 °C
Test cycle 3	10% O_2, 5% H_2O, 200 ppm NO and N_2 balance	10 °C/min ramp to 600 °C
H_2 treatment	5% H_2 and N_2 balance	600 °C
Test cycle 4	10% O_2, 5% H_2O, 200 ppm NO and N_2 balance	10 °C/min ramp to 600 °C
O_2 treatment	10% O_2 and N_2 balance	600 °C
Test cycle 5	10% O_2, 5% H_2O, 200 ppm NO and N_2 balance	10 °C/min ramp to 600 °C

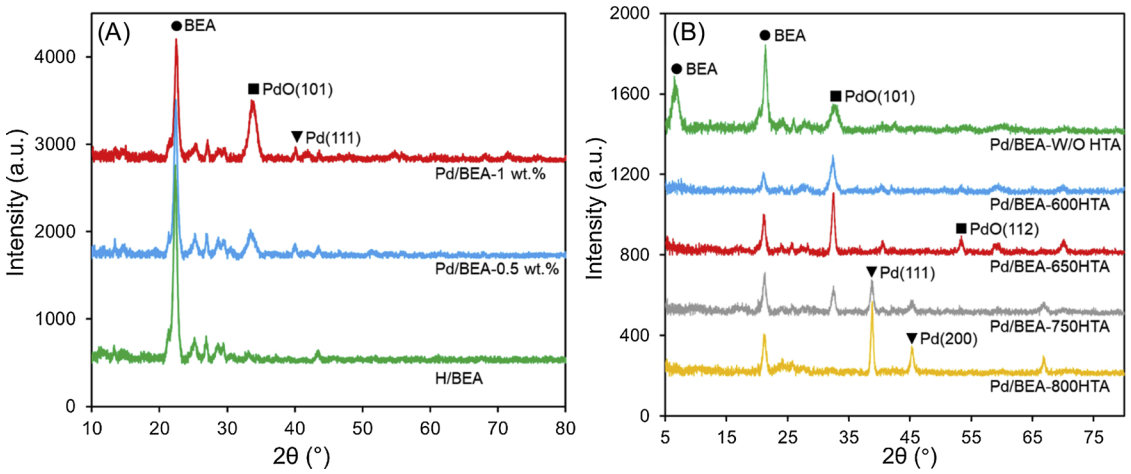

Fig. 1. Powder form XRD patterns of Panel A: H-BEA, 0.5 wt.% Pd/BEA and 1 wt.% Pd/BEA. Panel B: 1 wt.% Pd/BEA samples after different hydrothermal aging temperatures: 500 °C freshly calcined (Pd/BEA-W/O HTA) and 600 °C (Pd/BEA-600HTA), 650 °C (Pd/BEA-650HTA), 750 °C (Pd/BEA-750HTA), and 800 °C hydrothermally aged (Pd/BEA-800HTA).

relative to Pd/BEA-600HTA. The NOx-to-Pd ratio based on the amount adsorbed, listed in the figure, is 0.57 whereas after 600 °C hydrothermally aging it was 0.32. Furthermore, peak areas at 100–120 °C and 430 °C in the TPD profile increased. A similar hydrothermal aging effect has been reported in the literature for Pd/SSZ-13, where Ryou et al. showed that after hydrothermal aging a new NOx desorption feature appeared with a significant increase in NOx storage capacity [37]. It was concluded that the hydrothermal treatment helped disperse the Pd within the system and thus boosted the ion-exchange level [36]. Although Pd/BEA is a different system, the natures of the Pd species are believed to be similar, which will be further discussed with the H_2-TPR results later. Following the same testing protocol as that for Pd/BEA-600HTA, two consecutive NO and CO co-adsorption experiments were conducted. As shown in Fig. 2 **B**, when CO was present, the desorption temperature of the more weakly bound species, again, shifted to higher temperature. However, the desorption feature originally located at 180 °C appeared to broaden and its peak temperature shifted to 220 °C. Subsequent repetitions exhibited no variation. After NO and CO co-adsorption a NO adsorption probe experiment was used to see if CO changed the distribution of storage sites. Interestingly, even after only two adsorption experiments with CO, there was a loss of NOx storage capacity as evidenced by the elimination of peak at 430 °C and the decreased peak area at 100–120 °C. Therefore, unlike the Pd/BEA-600HTA sample, there was an irreversible change after CO exposure.

Atomically dispersed Pd cationic species are believed to be the most efficient NOx storage sites [27,38,39,45]. From the comparison of the 600 and 750 °C hydrothermally treated samples, the 750 °C treatment provided an initially higher ion-exchange level, however, the increase in NOx storage capacity was vulnerable to CO exposure, as the NOx storage capacity decreased after 2 cycles of NO and CO co-adsorption and TPD. The NO probe experiment after the CO exposure TPD profiles of both Pd/BEA-600HTA and Pd/BEA-750HTA appear similar to the fresh profiles, although the amount of NOx adsorbed on the Pd/BEA-750HTA decreased. One of the possible reasons to explain the decreased ion-exchange level is the CO reduction of Pd^{2+} species leading to Pd particle formation and growth, which has been reported by Ryou et al [41]. Although all the experiments here were conducted under lean conditions, complete CO oxidation is not achieved > 200 °C, as is shown in **Fig. S3**. Therefore, during the adsorption phase and TPD to at least 200 °C, CO is available to reduce Pd^{2+} species.

H_2-TPR was used to understand the nature of the Pd. Two consecutive H_2-TPR runs were performed on the 600 and 750 °C hydrothermally aged samples and the data are plotted in Fig. 3 **A**. TPR profiles of both Pd/BEA-600HTA and Pd/BEA-750HTA fresh samples (solid

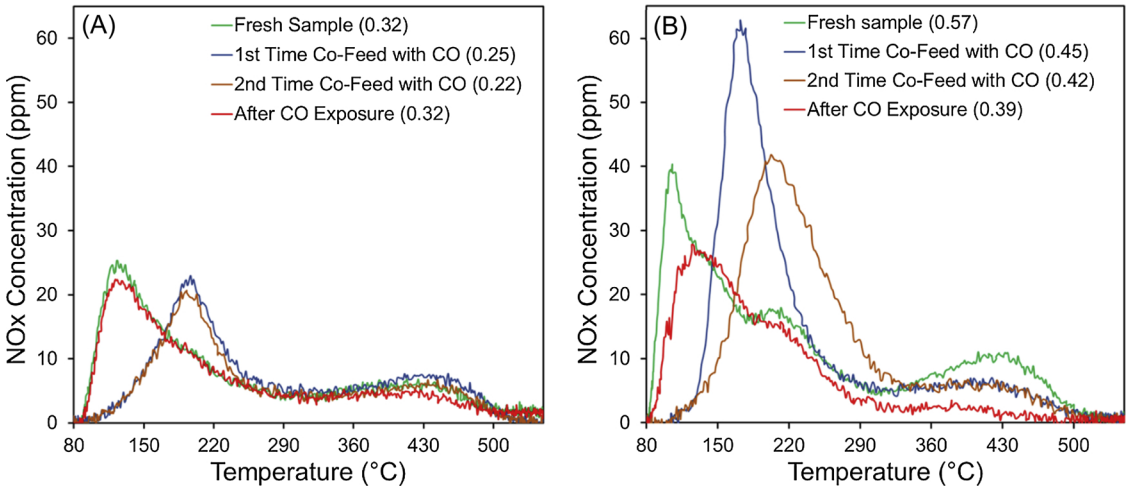

Fig. 2. NOx TPD profiles of consecutive NOx storage test cycles. Fresh sample and After CO Exposure storage tests were performed with 200 ppm NO, 5% H_2O and 10% O_2. 1st Time Co-Feed with CO and 2nd Time Co-Feed with CO tests were performed with 200 ppm CO, 200 ppm NO, 5% H_2O and 10% O_2. Samples used were **(A)** Pd-BEA-600HTA, **(B)** Pd-BEA-750HTA.

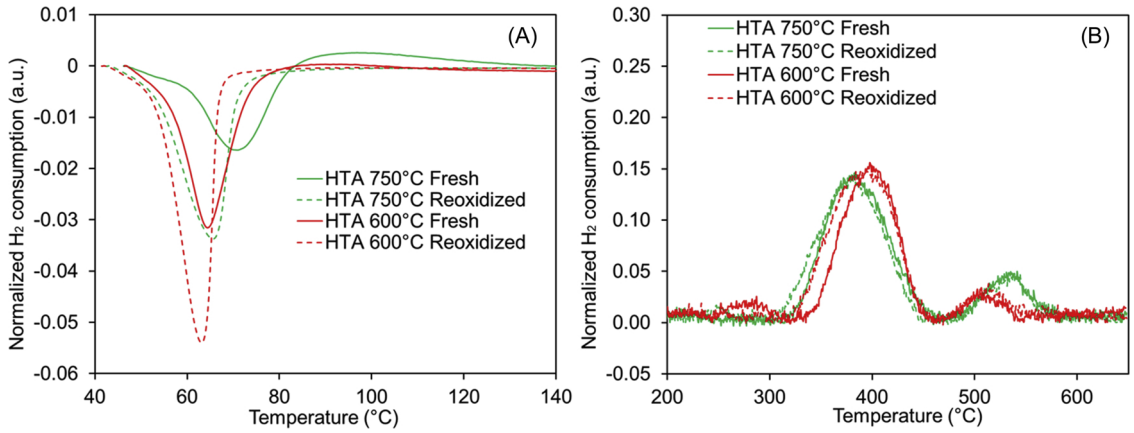

Fig. 3. Low temperature region (A) and high temperature region (B) H_2-TPR profiles of hydrothermally-treated samples (solid) and the results from an immediate repetition using the same sample after an O_2 pretreatment (dashed). Sample hydrothermal aging temperatures were: 600 and 750 °C.

lines) consist of two main features in the low temperature region: a negative peak at around 60 °C due to the decomposition of PdH (H_2 is generated) and a positive peak at around 100 °C associated with the reduction of Pd^{2+} to metallic Pd (H_2 is consumed). The Pd^{2+} reduction feature of Pd/BEA-600HTA is not as large as the Pd^{2+} reduction feature of Pd/BEA-750HTA. This result supports the conclusion drawn from the NOx adsorption and TPD comparison, where the initial ion-exchange level of Pd/BEA-750HTA is higher. In the high temperature region shown in Fig. 3 **B**, another reduction feature at 400 °C and a shoulder at 550 °C are observed for both Pd/BEA-750HTA and Pd/BEA-600HTA samples. These features are attributed to the reduction of a more stable ion-exchanged Pd species, of which the oxidation state has not been reported thus is denoted as Pd^{n+} in this work. Notably, the peak area of the Pd^{n+} reduction features for both Pd/BEA-750HTA and Pd/BEA-600HTA samples are similar, which suggests the same amount of Pd^{n+} exists in both samples.

After H_2-TPR, Pd cationic species are reduced to metallic Pd and it has been reported that a high temperature oxidative pretreatment is able to regenerate Pd cations in Pd/NaY after reduction [46,47]. To assess similarity with the Pd/BEA system, H_2-TPR was repeated after an oxidative pretreatment at 600 °C, and these results are shown as dashed lines in Fig. 3. The Pd^{2+} reduction feature of both samples disappeared and there was a more significant PdH decomposition peak in both cases. This suggests that after H_2 reduction at 600 °C, the reduced Pd^{2+} was not regenerated by the oxidative pretreatment and based on the larger PdH peak, bigger Pd particles formed. However, the reduction feature at 400–550 °C for both samples after the oxidative pretreatment are identical to the ones of the fresh samples, indicating the complete regeneration of what we have tentatively labelled Pd^{n+}. Although H_2 reduction is different from CO reduction in terms of their corresponding reaction mechanisms, CO has been reported to be a better reductant in reducing Pd in Pd/SSZ-13, i.e. it reduces Pd and causes particle agglomeration more easily, due to the enhanced mobility of Pd-carbonyl species [41].

To further investigate the characteristics of this irreversible degradation mode, Pd/BEA samples hydrothermally aged at other temperatures were also evaluated. NOx-to-Pd ratios before and after CO exposure are quantified and shown in Fig. 4 as “Fresh sample” and “CO exposed”. All samples except Pd/BEA-600C suffer from the irreversible degradation caused by CO exposure and their post−CO exposure NOx-to-Pd ratios are all around 0.3. It is also worth mentioning that the NOx-to-Pd ratios of the fresh samples followed the same trend reported in the Pd/SSZ-13 system, thus it is believed that the hydrothermal aging effect on Pd distribution is consistent within these two different Pd-zeolite systems.

Apart from fresh and CO-exposed samples, the NOx storage capacity of H_2-reduced and O_2-reoxidized samples were also measured and

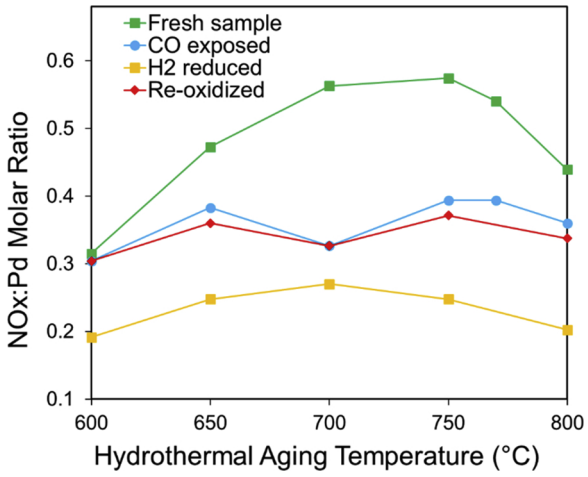

Fig. 4. NOx:Pd molar ratios of hydrothermally-treated samples (fresh), samples that were used for three cycles of NO and CO co-adsorption (CO exposed), samples reduced by H_2 at 600 °C following three NO and CO co-adsorption cycles (H2 reduced) and samples pretreated by O_2 at 600 °C following H_2 reduction at 600 °C (Re-oxidized).

shown in Fig. 4. Interestingly, H_2 reduced samples store the least NOx and an oxidative pretreatment regenerated the NOx storage capacity to post−CO exposure levels. This quantification result is consistent with the H_2-TPR result where loss of Pd^{2+} and regeneration of Pd^{n+} are observed when comparing the fresh and reoxidized TPR profiles. In other words, H_2 pretreatment at 600 °C reduced Pd^{n+} leading to a further decrease of the NOx storage capacity, but which can be regenerated by an O_2 pretreatment at 600 °C, shown as H_2-reduced and Re-oxidized in Fig. 4. Interestingly, though the total loss of cationic Pd species was observed in H_2O free H_2-TPR, a total loss in NOx storage capacity was not observed as is shown in **Fig. S.2 B**. This indicates that as soon as the catalyst is exposed to the O_2 and H_2O containing gas stream after H_2 reduction at 600 °C, part of the NOx storage capacity can be regenerated. Pd^{2+} was reduced by CO during NOx adsorption and TPD experiments at temperatures lower than 200 °C. The regeneration of Pd^{n+} thus appears facilitated by the presence of H_2O and O_2.

Although it has been reported that CO is able to readily reduce Pd cations [48] and it has been proven that high temperature H_2 reduction leads to loss of cations [41], the link between the reduced NOx storage capacity and the loss of Pd^{2+} as the CO vulnerable storage sites has not been established. Moreover, whether the loss of Pd^{2+} happens at elevated temperature where CO oxidation has achieved 100% conversion

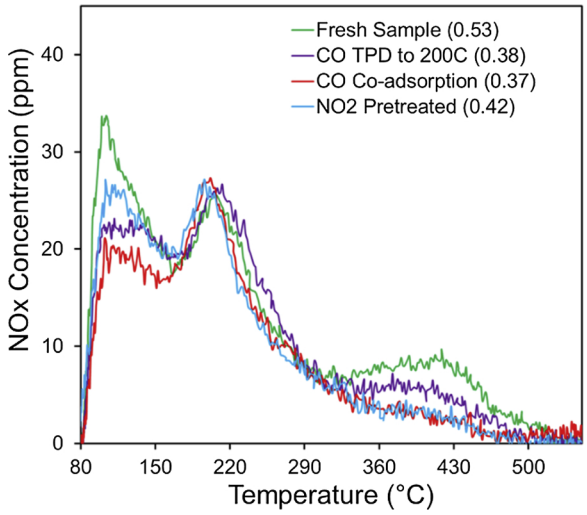

Fig. 5. NOx-TPD profiles of the 750 °C hydrothermally-treated sample, after being exposed to CO at 80 °C followed by a TPD to 200 °C, after three cycles of NO and CO co-adsorption and TPD, and after being treated by NO_2 following NO CO co-adsorption and TPD cycles. Numbers in the parentheses are NOx-to-Pd ratios.

or at low temperatures where CO oxidation has not lit off remains unresolved. This can be an important factor in determining the after-treatment design, as the first case, CO completely converted, can be avoided by integrating a diesel oxidation catalyst (DOC). However, the latter case, CO available, cannot because of the limited CO oxidation activity of DOCs at low temperatures. To further look into the mechanism of this irreversible loss of NOx storage degradation, a 750 °C hydrothermally treated sample was exposed to CO at 80 °C for 20 min followed by a temperature programmed desorption (TPD) to 200 °C, where the adsorbed CO is all released, after which an NO adsorption followed by TPD experiment was performed. The TPD profile is shown in Fig. 5 labeled as "CO TPD to 200 C". Also, a CO-exposed Pd/BEA-750HTA sample was exposed to a regeneration gas mixture consisting of 1500 ppm NO_2, 800 ppm NO and 15% of O_2 balanced by N_2, which has been reported to selectively regenerate Pd^{2+} from PdOx particles via accelerated protonolysis [44]. After a 24 -h NO_2 regeneration, the same NO adsorption/TPD probe experiment was again performed, and the TPD profile is shown as "NO2 regenerated" in Fig. 5 together with TPD profiles of fresh and CO-exposed Pd/BEA-750HTA samples. Details of the experiment procedure are listed in Table 2. H_2-TPR profiles from all four different states are also shown in Fig. 6 for comparison. CO exposure and NO_2 regeneration only affected the desorption features at 100 and 430 °C whereas the peak at 200 °C remained unaffected. Their corresponding Pd^{2+} reduction features in H_2-TPR profiles are proportional to the NOx uptake measured from NO adsorption experiments. This supports the hypothesis that the loss of NOx storage capacity is explicitly attributed to the irreversible loss of Pd^{2+} caused by CO exposure, more importantly, CO exposure at temperatures no higher than 200 °C already led to Pd^{2+} reduction. However, CO nears 100% conversion at ~200 °C and therefore the reduction of Pd^{2+} only occurs during the adsorption phase and the initial part of the TPD. Hence, for one adsorption and desorption cycle, a limited time is available to facilitate the degradation, which is why changes in the NOx storage capacity as well as the NOx TPD profile were observed during the first repeats of the NO and CO co-adsorption experiments, and eventually reached a stable state.

As discussed previously, NOx TPD profiles of almost all fresh samples consist of three NOx desorption features indicating at least three different types of surface intermediates or 3 different storage sites. NO interacting with/adsorbing onto Bronsted acid sites can be eliminated due to the presence of H_2O [27]. Moreover, Pd and PdOx particles are

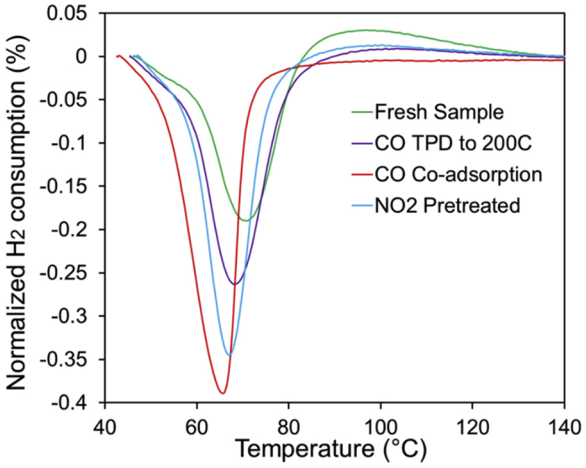

Fig. 6. H_2-TPR profiles of the 750 °C hydrothermally-treated sample, after being exposed to CO at 80 °C followed by a TPD to 200 °C, after three cycles of NO and CO co-adsorption and TPD, and after being treated by NO_2 following NO CO co-adsorption and TPD cycles.

believed to be unable to uptake NOx [49]. Therefore, Pd cationic species are assumed to be responsible for low temperature NOx storage in our Pd/BEA system, of which, a certain type of Pd^{2+} is vulnerable to CO exposure even under lean conditions, and what has been labelled as Pd^{n+} can be easily regenerated with the presence of H_2O and O_2 even at 80 °C. To assess the identity and the structure of the CO vulnerable Pd^{2+} species, the amount of H_2 associated with the Pd^{2+} reduction feature was quantified from H_2-TPR results as was the amount of stored NOx associated with the vulnerable Pd^{2+} species from NOx-TPD results. Fig. 7 suggests that they follow a linear relationship with a NOx-to-Pd ratio of 0.5.

3.3. HAADF-STEM

In addition to the characterization of Pd/BEA samples by H_2-TPR, TEM was used to image the unexchanged Pd nanoparticles that reside on the external surface and outside the zeolite cages. As shown in Fig. 8, STEM images of Pd/BEA calcined at 500 °C **(A)**, hydrothermally aged at 750 °C **(B)**, H_2 reduced at 600 °C **(C)**, and CO-exposed Pd/BEA **(D)** all show the existence of Pd particles. Due to the incomplete ion-exchange

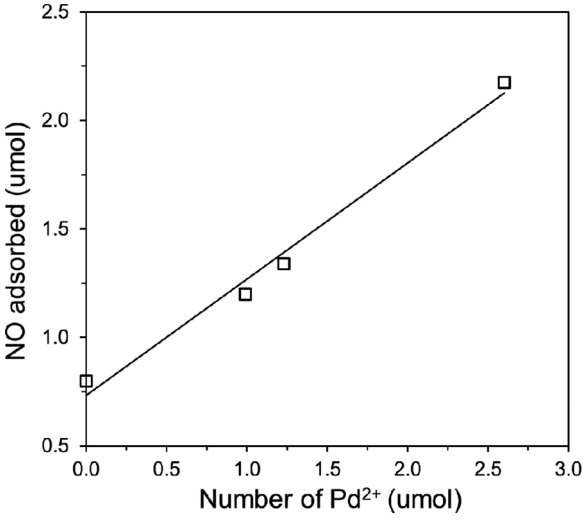

Fig. 7. Correlation between NO adsorbed and Pd^{2+}. NO adsorbed was calculated from NO adsorption uptake, and the Pd^{2+} amount was calculated from the integration of the 100 °C reduction feature in the H_2-TPR experiment shown in Fig. 6.

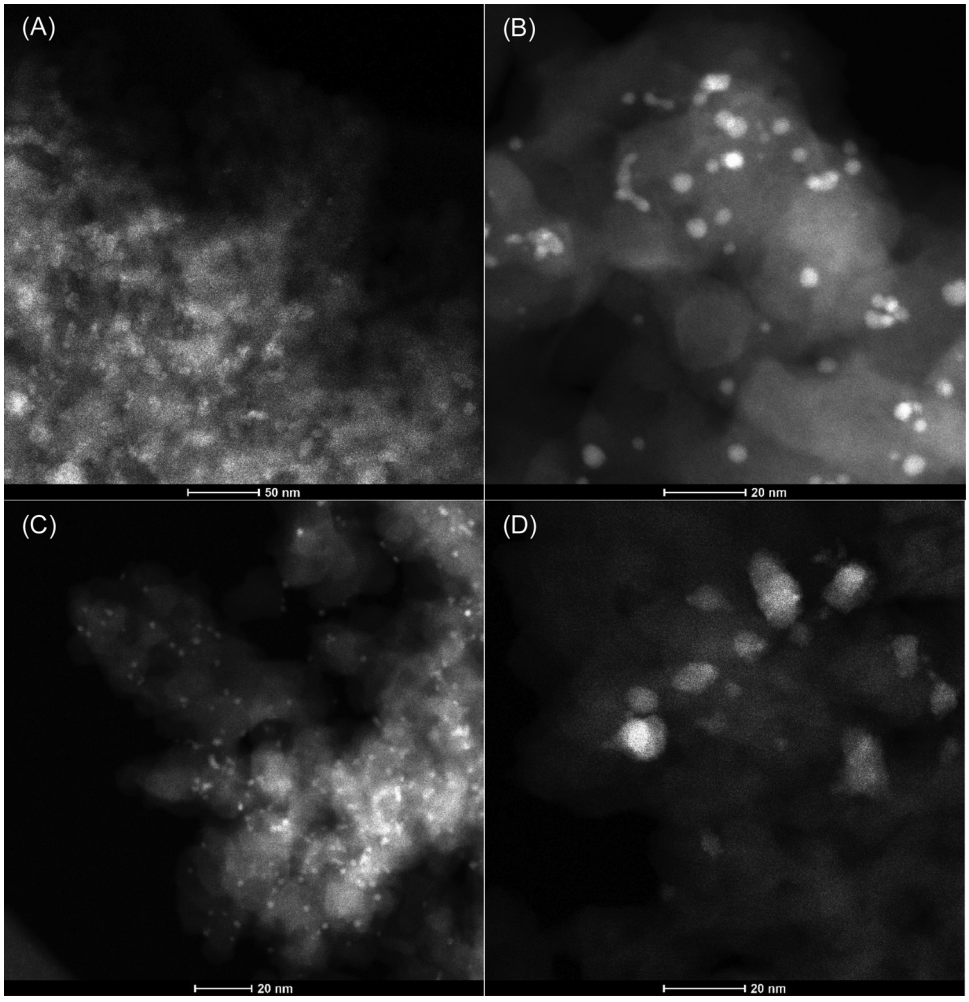

Fig. 8. STEM images of **(A)** a freshly calcined Pd/BEA; **(B)** Pd/BEA-750HTA after O_2 pretreatment at 600 °C; **(C)** Pd/BEA-750HTA after H_2 pretreatment at 600 °C; **(D)** Pd/BEA-750HTA after CO exposure.

of the freshly calcined sample, Pd particles are present throughout the selected area in Fig. 8 **A**. After the calcination process, the average particle size was around 5 nm, and based on the NOx adsorption and H_2 TPR results, most of the Pd particles locate on the zeolite external surface due to the limited pore opening of BEA structure. The average Pd particle size increased after hydrothermal aging at 750 °C, as shown in Fig. 8 **B**. This may appear to contradict the increase in the NOx storage capacity, but in fact, some Pd can diffuse into the zeolite and reach a Bronsted acid site to facilitate protonolysis, which results in a higher ion-exchange level [36,37,44]. Therefore, Pd particle agglomeration and ion-exchange via protonolysis happened simultaneously during hydrothermal aging. A NOx storage capacity increase has also been observed for Pd/SSZ-13 [36,37] and protonolysis was mechanistically proven for a Pd/NaY model catalyst [44]. Notably, protonolysis is an activated and particle size dependent process, that is, if the Pd particle size is too large the activation energy of the protonolysis process will be too high to compete with particle agglomeration [44]. However, particle agglomeration was not observed for Pd/SSZ-13 and Pd/ZSM-5 and a possible explanation could be the larger pore opening of Pd/BEA allowing bigger particles to form. The STEM image of a H_2-reduced Pd/BEA sample is shown in Fig. 8 **C**, and interestingly, a significant amount of Pd particles ranging from 2 to 3 nm are evident. This could be due to the reduction of atomically dispersed Pd cationic species and insufficient time for particles to agglomerate. Finally, a STEM image of a CO-exposed Pd/BEA sample is shown in Fig. 8 **D**, and significantly larger Pd particles are evident with an average particle size around 12 nm. CO, as a key component of diesel exhaust, has been proven to accelerate Pd particle agglomeration by itself under rich conditions [41]. Notably, for all the NO and CO co-adsorption and TPD experiments, near 100% CO conversion was achieved at temperatures ~200 °C, in other words the highest CO exposure temperature is around 200 °C. Therefore, the comparison of Fig. 8 **D** and Fig. 8 **B** suggests that during the NO and CO co-adsorption experiment, Pd particles become significantly larger. Meanwhile, H_2-TPR results from the same samples showed a decreased amount of Pd^{2+} after CO exposure. This suggests a two-step process, the reduction of Pd^{2+} by CO generating small Pd particles and then these small particles agglomerate preventing Pd from being ion-exchanged back into the zeolite framework. Herein, we attribute the irreversible loss of the NOx storage capacity to this Pd redistribution process.

4. Conclusions

Pd/BEA passive NOx adsorbers were evaluated for low-temperature NOx adsorption and NOx release, using adsorption and TPD experiments. The results revealed the mechanism of an irreversible degradation mode caused by CO exposure. H_2-TPR and the TPD experiments show that different Pd cationic species exist within the Pd/BEA system and are NOx storage sites, part of which are also vulnerable to degradation via CO exposure. H_2-TPR and STEM imaging showed that CO exposure at temperatures lower than 200 °C leads to an irreversible loss of Pd^{2+} due to a two-step Pd^{2+} reduction and particle agglomerating

process. And CO plays an important role in accelerating the particle agglomeration. We speculate that another Pd cationic species also contributes to NOx storage and is less vulnerable to CO or reductant as its reduction can be reversed. The irreversible NOx storage degradation can be partially regenerated by a long duration NO_2 exposure. Overall, to slow a Pd/BEA PNA degradation via CO exposure, a highly active DOC is necessary, additionally, NO_2 generated from DOC can also lead to regeneration of NOx storage via accelerated protonolysis.

Acknowledgements

The authors gratefully acknowledge support from the Department of Energy, Vehicle Technologies Office (DE- EE0008233).

Appendix A. Supplementary data

Supplementary material related to this article can be found, in the online version, at doi:https://doi.org/10.1016/j.apcatb.2019.118032.

References

[1] S. Matsumoto, Recent advances in automobile exhaust catalysts, Catal. Today 90 (2004) 183–190.
[2] A.M. Beale, F. Gao, I. Lezcano-Gonzalez, C.H.F. Peden, J. Szanyi, Recent advances in automotive catalysis for NO x emission control by small-pore microporous materials, Chem. Soc. Rev. 44 (2015) 7371–7405.
[3] H.C. Frey, Trends in onroad transportation energy and emissions, J. Air Waste Manage. Assoc. 68 (2018) 514–563.
[4] T. Johnson, Vehicular emissions in review, SAE Int. J. Engines. 9 (2016) 2016-01–0919.
[5] B.T. Johnson, Diesel engine emissions and their control, Platin. Met. Rev. 52 (2008) 23–37.
[6] M.V. Twigg, Progress and future challenges in controlling automotive exhaust gas emissions, Appl. Catal. B Environ. 70 (2007) 2–15.
[7] F. Gao, Y. Wang, M. Kollár, N.M. Washton, J. Szanyi, C.H.F. Peden, A comparative kinetics study between Cu/SSZ-13 and Fe/SSZ-13 SCR catalysts, Catal. Today 258 (2015) 347–358.
[8] P. Forzatti, I. Nova, E. Tronconi, New “Enhanced NH 3 -SCR” reaction for NOx emission control, Ind. Eng. Chem. Res. 49 (2010) 10386–10391.
[9] D. Wang, Y. Jangjou, Y. Liu, M.K. Sharma, J. Luo, J. Li, K. Kamasamudram, W.S. Epling, A comparison of hydrothermal aging effects on NH 3 -SCR of NO x over Cu-SSZ-13 and Cu-SAPO-34 catalysts, Appl. Catal. B Environ. 165 (2015) 438–445.
[10] Y. Jangjou, Q. Do, Y. Gu, L.-G. Lim, H. Sun, D. Wang, A. Kumar, J. Li, L.C. Grabow, W.S. Epling, Nature of Cu active centers in Cu-SSZ-13 and their responses to SO 2 exposure, ACS Catal. 8 (2018) 1325–1337.
[11] J.A. Loiland, R.F. Lobo, Oxidation of zeolite acid sites in NO/O 2 mixtures and the catalytic properties of the new site in NO oxidation, J. Catal. 325 (2015) 68–78.
[12] C. Sharp, C.C. Webb, S. Yoon, M. Carter, C. Henry, Achieving ultra low NOX emissions levels with a 2017 heavy-duty on-highway TC diesel engine - comparison of advanced technology approaches, SAE Int. J. Engines. 10 (2017) 2017-01–0956.
[13] M. Moliner, A. Corma, From metal-supported oxides to well-defined metal site zeolites: the next generation of passive NO x adsorbers for low-temperature control of emissions from diesel engines, React. Chem. Eng. (2019).
[14] J. Lee, J.R. Theis, E.A. Kyriakidou, Vehicle emissions trapping materials: successes, challenges, and the path forward, Appl. Catal. B Environ. 243 (2019) 397–414.
[15] V. Schmeisser, M. Weibel, L. Sebastian Hernando, I. Nova, E. Tronconi, M.P. Ruggeri, Cold start effect phenomena over zeolite SCR catalysts for exhaust gas after treatment, SAE Int. J. Commer. Veh. 6 (2013) 190–199.
[16] Y. Gu, W.S. Epling, Passive NOx adsorber: an overview of catalyst performance and reaction chemistry, Appl. Catal. A Gen. 570 (2019) 1–14.
[17] H.-Y. Chen, D. Liu, E. Weigert, L. Cumaranatunge, K. Camm, P. Bannon, J. Cox, L. Arnold, Durability Assessment of Diesel Cold Start Concept (dCSC™) Technologies, SAE Int. J. Engines. 10 (2017) 2017-01–0955.
[18] H.-Y. Chen, S. Mulla, E. Weigert, K. Camm, T. Ballinger, J. Cox, P. Blakeman, Cold Start Concept (CSC™): A Novel Catalyst for Cold Start Emission Control, SAE Int. J. Fuels Lubr. 6 (2013) 2013-01–0535.
[19] S. Jones, Y. Ji, A. Bueno-Lopez, Y. Song, M. Crocker, CeO2-M2O3 passive NOx adsorbers for cold start applications, Emiss. Control Sci. Technol. 3 (2017) 59–72.
[20] Y. Ji, D. Xu, S. Bai, U. Graham, M. Crocker, B. Chen, C. Shi, D. Harris, D. Scapens, J. Darab, Pt- and Pd-Promoted CeO2 –ZrO2 for passive NOx adsorber applications, Ind. Eng. Chem. Res. 56 (2017) 111–125.
[21] S. Jones, Y. Ji, M. Crocker, Ceria-based catalysts for low temperature NOx storage and release, Catal. Letters 146 (2016) 909–917.
[22] Y. Ji, S. Bai, M. Crocker, Al2O3-based passive NOx adsorbers for low temperature applications, Appl. Catal. B Environ. 170–171 (2015) 283–292.
[23] J.R. Theis, C.K. Lambert, An assessment of low temperature NOx adsorbers for cold-start NOx control on diesel engines, Catal. Today 258 (2015) 367–377.
[24] J.R. Theis, C.K. Lambert, Mechanistic assessment of low temperature NO x adsorbers for cold start NO x control on diesel engines, Catal. Today 258 (2017) 367–377.
[25] J.R. Theis, C. Lambert, The effects of CO, C_2H_4, and H_2O on the NO_x storage performance of low temperature NO_x adsorbers for diesel applications, SAE Int. J. Engines. 10 (2017) 2017-01–0942.
[26] Y. Ji, D. Xu, M. Crocker, J.R. Theis, C. Lambert, A. Bueno-Lopez, D. Harris, D. Scapens, Mn-based mixed oxides for low temperature NOx adsorber applications, Appl. Catal. A Gen. 567 (2018) 90–101.
[27] H.-Y. Chen, J.E. Collier, D. Liu, L. Mantarosie, D. Durán-Martín, V. Novák, R.R. Rajaram, D. Thompsett, Low temperature NO storage of zeolite supported Pd for low temperature diesel engine emission control, Catal. Letters 146 (2016) 1706–1711.
[28] O. Mihai, L. Trandafilović, T. Wentworth, F.F. Torres, L. Olsson, The effect of Si/Al ratio for Pd/BEA and Pd/SSZ-13 used as passive NOx adsorbers, Top. Catal. 0 (2018) 0.
[29] S. Ren, S.J. Schmieg, C.K. Koch, G. Qi, W. Li, Investigation of Ag-based low temperature NOx adsorbers, Catal. Today 258 (2015) 378–385.
[30] J. Lee, Y. Ryou, S.J. Cho, H. Lee, C.H. Kim, D.H. Kim, Investigation of the active sites and optimum Pd/Al of Pd/ZSM–5 passive NO adsorbers for the cold-start application: evidence of isolated-Pd species obtained after a high-temperature thermal treatment, Appl. Catal. B Environ. 226 (2018) 71–82.
[31] A. Porta, T. Pellegrinelli, L. Castoldi, R. Matarrese, S. Morandi, S. Dzwigaj, L. Lietti, Low temperature NOx adsorption study on Pd-Promoted zeolites, Top. Catal. 0 (2018) 0.
[32] Y. Zheng, L. Kovarik, M.H. Engelhard, Y. Wang, Y. Wang, F. Gao, J. Szanyi, Low-Temperature Pd / Zeolite Passive NOx Adsorbers : Structure, Performance and Adsorption Chemistry Low-Temperature Pd / Zeolite Passive NOx Adsorbers : Structure, Performance and Adsorption Chemistry Abstract, (2017), pp. 1–10.
[33] J. Lee, Y. Ryou, S. Hwang, Y. Kim, S.J. Cho, H. Lee, C.H. Kim, D.H. Kim, Comparative study of the mobility of Pd species in SSZ-13 and ZSM-5, and its implication for their activity as passive NO x adsorbers (PNAs) after hydro-thermal aging, Catal. Sci. Technol. 9 (2019) 163–173.
[34] D. Mei, F. Gao, J. Szanyi, Y. Wang, Mechanistic insight into the passive NOx adsorption in the highly dispersed Pd/HBEA zeolite, Appl. Catal. A Gen. 569 (2019) 181–189.
[35] Y. Zheng, L. Kovarik, M.H. Engelhard, Y. Wang, Y. Wang, F. Gao, J. Szanyi, Low-Temperature Pd/Zeolite Passive NO x Adsorbers: Structure, Performance, and Adsorption Chemistry, J. Phys. Chem. C. 121 (2017) 15793–15803.
[36] Y. Ryou, J. Lee, H. Lee, C.H. Kim, D.H. Kim, Effect of various activation conditions on the low temperature NO adsorption performance of Pd/SSZ-13 passive NOx adsorber, Catal. Today 320 (2019) 175–180.
[37] Y. Ryou, J. Lee, S.J. Cho, H. Lee, C.H. Kim, D.H. Kim, Activation of Pd/SSZ-13 catalyst by hydrothermal aging treatment in passive NO adsorption performance at low temperature for cold start application, Appl. Catal. B Environ. 212 (2017) 140–149.
[38] K. Khivantsev, N.R. Jaegers, L. Kovarik, J.C. Hanson, F.F. Tao, Y. Tang, X. Zhang, I.Z. Koleva, H.A. Aleksandrov, G.N. Vayssilov, Y. Wang, F. Gao, J. Szanyi, Achieving atomic dispersion of highly loaded transition metals in small-pore zeolite SSZ-13: a new class of high-capacity and high-efficiency low temperature CO and NOx adsorbers, Angew. Chemie. (2018).
[39] K. Khivantsev, F. Gao, L. Kovarik, Y. Wang, J. Szanyi, Molecular level understanding of how oxygen and carbon monoxide improve NOx storage in Palladium/SSZ-13 passive NO x adsorbers: the role of NO+ and Pd(II)(CO)(NO) species, J. Phys. Chem. C. 122 (2018) 10820–10827.
[40] A. Vu, J. Luo, J. Li, W.S. Epling, Effects of CO on Pd/BEA passive NOx adsorbers, Catal. Letters 147 (2017) 745–750.
[41] Y. Ryou, J. Lee, Y. Kim, S. Hwang, H. Lee, C.H. Kim, H.K. Do, Effect of reduction treatments (H2 vs. CO) on the NO adsorption ability and the physicochemical properties of Pd/SSZ-13 passive NOx adsorber for cold start application, Appl. Catal. A Gen. (2018).
[42] A.K. Datye, J. Bravo, T.R. Nelson, P. Atanasova, M. Lyubovsky, L. Pfefferle, Catalyst microstructure and methane oxidation reactivity during the Pd↔PdO transformation on alumina supports, Appl. Catal. A Gen. 198 (2000) 179–196.
[43] M. Iwasaki, H. Shinjoh, Hydrothermal stability enhancement by sequential ion-exchange of rare earth metals on Fe/BEA zeolites used as NO reduction catalysts, Chem. Commun. (2011) 3966–3968.
[44] B.J. Adelmana, W.M.H. Sachtler, The effect of zeolitic protons on NO, reduction over Pd / ZSM-5 catalysts, Science (80-.) 14 (1997).
[45] K. Khivantsev, N.R. Jaegers, L. Kovarik, S. Prodinger, M.A. Derewinski, Y. Wang, F. Gao, J. Szanyi, Palladium/Beta zeolite passive NOx adsorbers (PNA): clarification of PNA chemistry and the effects of CO and zeolite crystallite size on PNA performance, Appl. Catal. A Gen. 569 (2019) 141–148.
[46] S.T. Homeyer, W.M.H. Sachtler, Oxidative redispersion of palladium and formation of PdO particles in NaY, Appl. Catal. 54 (1989) 189–202.
[47] S. Homeyer, Elementary steps in the formation of highly dispersed palladium in NaY I. Pd ion coordination and migration, J. Catal. 117 (1989) 91–101.
[48] A.W. Aylor, L.J. Lobree, J.A. Reimer, A.T. Bell, Investigations of the Dispersion of Pd in H-ZSM-5, J. Catal. 172 (1997) 453–462.
[49] M. Ogura, M. Hayashi, S. Kage, M. Matsukata, E. Kikuchi, Determination of active palladium species in ZSM-5 zeolite for selective reduction of nitric oxide with methane, Appl. Catal. B Environ. 23 (1999) 247–257.